TRENDS IN SCIENCES 2026; 23(8): 12908
https://doi.org/10.48048/tis.2026.12908
RESEARCH ARTICLE

Green Synthesis of Zinc Oxide Nanoparticles Using Fruit Peel Waste Extract of *Nypa fruticans* Via Microwave-Assisted as Antioxidant and Antibacterial Agents

Reza Destri Anggi[1], Diding Pradita[1], Adek Chan[1], Hanafis Sastra Winata[1], Mutiara Qisthina Hanif[2] and Muhammad Fauzan Lubis[3,*]

[1]*Department of Pharmacy, Faculty of Pharmacy and Medicine, Institut Kesehatan Helvetia, Medan 20124, Indonesia*
[2]*Eye Specialty Hospital Mencirim Tujuh Tujuh, Medan, North Sumatera 21054, Indonesia*
[3]*Department of Pharmaceutical Biology, Faculty of Pharmacy, Universitas Sumatera Utara, Medan 20155, Indonesia*

([*]Corresponding author's e-mail: fauzan.lubis@usu.ac.id)

Received: 6 December 2025, Revised: 5 January 2026, Accepted: 12 January 2026, Published: 15 March 2026

Abstract

Nanostructured particles exhibit broad applicability in nanotechnology-related fields, with their properties strongly influenced by the synthesis method and material source. This study reports an eco-friendly, microwave-assisted approach for synthesizing zinc oxide nanoparticles (ZnO NPs) using *Nypa fruticans* fruit peel extract (FPNP). The quantification of the total phenolic (TPC) and flavonoid content (TFC) of FPNP was determined using a calorimetric assay. Whereas, the biosynthesis of ZnO NPs-FPNP was characterized with several instrumental methods, including UV-Vis spectrophotometer, Fourier transform infrared spectroscopy (FT-IR), particle size and zeta potential analyzer (PSA and ZPA), scanning electron microscopy (SEM), transmission electron microscopy (TEM), energy-dispersive X-ray spectroscopy (EDX), x-ray diffraction (XRD), and thermogravimetric analysis (TGA). Therefore, the antioxidant and antibacterial activities of ZnO NPs-FPNP were observed to evaluate the biological activity of nanoparticles. Furthermore, the FPNP contains TPC and TFC were 20.53 ± 1.20 mg GAE/g and 15.80 ± 1.46 mg QE/g, respectively. Meanwhile, the ZnO NPs-FPNP was acquired as an amorphous yellowish-white powder, devoid of any discernible odour, and was comprehensively characterised. The visible spectra revealed a significant peak at 370 nm, correlating to a band gap energy of 3.04 eV, thus confirming the synthesis of the nanoparticles. FTIR spectra indicated that the peak at 497 cm^{-1} corresponds to the stretching vibration of Zn-O, which is the characteristic peak for the formation of ZnO NPs-FPNP. The particle size of ZnO NPs-FPNP, as determined by particle size analysis, is 234 ± 59.5 nm, with a polydispersity index of 0.516. The zeta potential of ZnO NPs-FPNP was measured at –25.7 ± 1.50 mV, signifying the stability of the ZnO NPs-FPNP. The SEM image displayed an uneven morphology, with primary particle sizes at the nanometre scale that tend to combine into micrometre clusters. TEM investigation revealed that ZnO NPs-FPNP predominantly exhibited a rod-like morphology, with lengths varying from approximately 50 to 150 nm and diameters between 20 and 40 nm. The ZnO NPs-FPNP were confirmed to comprise three elements: zinc, oxygen, and carbon. The XRD pattern confirmed that the ZnO NPs-FPNP have a wurtzite crystal structure, demonstrating significant stability at temperatures above 400 °C. This study exhibited that the no significant difference in the antioxidant activity to inhibit radical DPPH and ABTS between ascorbic acid and ZnO NPs-FPNP at the highest concentration. Then, the ZnO NPs-FPNP have demonstrated bactericidal effect against *Escherichia coli* and *Staphylococcus aureus*. Nonetheless, ZnO NPs-FPNP have potential applications in pharmaceuticals, cosmeceuticals, and agriculture.

Keywords: Zinc oxide nanoparticles, Nypa fruticans waste, Microwave irradiation, Antioxidant, Antibacterial

Introduction

Zinc oxide nanoparticles (ZnO NPs) have long been recognized for their significant biological effects, including their antibacterial and antioxidant properties [1]. The fact that conventional synthesis techniques for ZnO NPs usually require the use of hazardous chemicals and a substantial energy input raises concerns about the environmental impact [2]. Numerous studies have shown that using chemicals like sodium hydroxide and sodium borohydride as reducing agents in the synthesis of ZnO can result in the production of hazardous waste that is bad for the environment [3]. Furthermore, traditional synthesis methods frequently require high temperatures and lengthy reaction times, resulting in significant energy usage [4]. As a result, there has been a lot of research done on creating eco-friendly synthesis techniques using natural resources [5]. For instance, *Mallotus philippinensis* leaf extract was effectively used by Khajuria *et al*. [6] to biosynthesize ZnO, which demonstrated strong antibacterial properties [6]. In a similar vein, Abisha *et al*. [7] successfully synthesized ZnO NPs using plant extracts and a microwave-assisted technique, yielding tiny nanoparticles with strong antioxidant properties [7].

The fruit peel waste of the *Nypa fruticans* is one of the main potentials that has not been thoroughly investigated. The fruit peel of the *N. fruticans*, a mangrove plant that grows widely along Indonesia's coastline, is frequently thrown away as waste [8]. Nevertheless, early research has shown that the peel of *N. fruticans* fruit includes bioactive substances such as flavonoids and phenolics, which may act as organic stabilizing and reducing agents during the creation of nanoparticles [9]. Apart from its potential for bioactivity, this extract is well-suited for use in microwave-assisted biosynthesis. Rapid and even heating, accelerated nanoparticle production, and improved particle homogeneity are all made possible by the use of microwave irradiation in the synthesis process [10]. Microwaves' volumetric heating mechanism may greatly speed up the rate of reaction without the need for high temperatures or extended reaction times, which promotes an environmentally friendly green synthesis method [11].

The green synthesis approach utilizing *N. fruticans* fruit peel waste and microwave-assisted synthesis is expected to enhance the antioxidant and antibacterial effectiveness of the resulting ZnO NPs. This has previously been reported in several studies, such as those revealed by Hao *et al.* [12], that the antibacterial activity of ZnO NPs synthesized under microwave conditions is increased against *Staphylococcus aureus* [12]. A similar report by Mallikarjunaswamy *et al*. [13] demonstrated that the antioxidant and antibacterial activities of ZnO NPs synthesized under microwave using *Aegle marmelos* were elevated compared to non-microwave-assisted [13]. On the other hand, Acar *et al*. [14] showed that the biological activity of ZnO NPs synthesized under microwave using *Calendula officinalis* flower extract was improved [14]. Despite numerous studies on the green synthesis of ZnO NPs using various plant extracts, the utilization of *N. fruticans* fruit peel waste as a bioreductant and stabilizing agent remains scarcely explored, particularly under microwave-assisted conditions. Most existing studies focus on edible plant parts or conventional heating methods, with limited attention to waste valorization and rapid synthesis approaches. Therefore, this study addresses this research gap by employing *N. fruticans* fruit peel waste in a microwave-assisted green synthesis of ZnO nanoparticles and systematically evaluating their physicochemical properties, antioxidant capacity, and antibacterial activity. The integration of agricultural waste utilization with microwave-assisted nanomaterial synthesis represents the key novelty of this work and contributes to the development of sustainable nanotechnology for biomedical applications.

Materials and methods

Plant collection

The Phytochemistry Laboratory, Faculty of Pharmacy, Universitas Sumatera Utara, Indonesia, was the site of this investigation in April 2025. *N. fruticans* fruits were gathered from Medan Belawan's coastal region in North Sumatra, Indonesia. A botanist from Universitas Sumatera Utara's Herbarium Medanese subsequently recognized the fruit peels, and their authenticity as *N. fruticans* peel was verified and noted under Voucher ID: 345/HM-USU/2025. To obtain a consistent dry powder, the cleaned fruit peels were blended in a traditional blender, sieved, and dried in a drying cabinet. Before being used in the biosynthetic

process, the dry powdered *N. fruticans* fruit peel was kept in an airtight container.

Plant extraction and determination of phytochemical content

The fruit peel of *N. fruticans* was extracted via infusion. An Erlenmeyer flask containing 10 g of dried powder was filled with 100 mL of boiling water. For 30 min, the mixture was heated to 80 °C. To improve solvent penetration and ease the release of bioactive chemicals from the sample, the mixture was agitated while it was heating. Filtration was used to stop the extraction process, and the filtrate was gathered. The filtrate was used within 24 h after being kept in a glass bottle that was tightly sealed [15]. First, the Folin-Ciocalteu reagent was used to measure the aqueous extract's total phenolic content (TPC). In short, a UV-Vis spectrophotometer set to 765 nm wavelength was used to measure the color that resulted from the extract's reaction with Folin-Ciocalteu. The TPC of the sample was quantified by absorbance measurements and reported as gallic acid (GA) equivalents (mg GAE/g sample) [16]. The extract was then reacted with aluminum chloride to assess the aqueous extract's total flavonoid concentration (TFC). A UV-Vis spectrophotometer set at 415 nm was used to measure the resultant color. The number of quercetin (Q) equivalents (mg QE/g sample) was used to determine the TFC of the sample [17].

Biosynthesis of zinc oxide nanoparticles

A volume of 50 mL of *N. fruticans* fruit peel extract (FPNP) was amalgamated with 50 mL of a solution of zinc nitrate hexahydrate (0.1 M), which was subjected to continuous agitation. with a magnetic stirrer for 10 min at room temperature. It was mixed with NaOH (1 M) until the pH level hit 10 - 11. After that, the reaction mixture was exposed to 800 W of microwave radiation for 10 min in cycles of 30 s ON and 30 s OFF. Following irradiation, the mixture was centrifuged for 10 min at 8,000 rpm after being left to remain at room temperature for 15 to 30 min. It was cleaned twice with water that had minerals taken out, and then it was dried in an oven at 60 °C for 24 h. Before being characterized and assessed, the powdered ZnO NPs-FPNP were kept at room temperature in a dark glass container [18-20].

Characterization of zinc oxide nanoparticles

Several techniques were used to characterize ZnO NPs-FPNP. These included using UV-Vis spectrophotometry to determine the absorption peak position of the formed ZnO NPs-FPNP and bandgap energy following Eq. (1). FTIR to identify functional groups, zeta potential analyzer (ZPA) and particle size analyzer (PSA) to measure the zeta potential energy, hydrodynamic particle size (PS), and polydispersity index (PI), SEM, TEM, and EDX to observe surface morphology and elemental composition, XRD to identify ZnO crystals and the size of crystal according to the Eq. (2). Therefore, DTG to assess thermal stability and volatile content [5,21-25].

$$\mathrm{Eg} = \frac{hc}{\lambda} \quad (1)$$

where *'Eg'* is bandgap energy, h is Planck's constant 6.626×10^{-36} J·s, *'c'* is speed of light 3.8×10^{8} m/s, and 'λ' is absorption wavelength.

$$\mathrm{D} = \left(\frac{K\lambda}{\beta Cos\theta}\right)\mathrm{A}^{\circ} \quad (2)$$

where D is the average crystallite diameter in Angstrom, K is the Scherrer constant, λ is the wavelength of X-ray, i.e., 1.5406 Å, CuKα radiation, Θ is the Bragg's angle, and β is the full width at half maximum intensity of the diffraction peak.

Antioxidant activity of zinc oxide nanoparticles

These tests were DPPH and ABTS radical scavenger experiments used to assess the antioxidant activity of ZnO NPs-FPNP. Briefly, a DPPH solution was combined with ZnO NPs-FPNP at different doses between 31.25 to 500 µg/mL for the DPPH assay. It was measured at 517 nm after the mixes were left to sit at room temperature for 30 min in the dark. Whereas, by combining samples at different concentrations (31.25 to 500 µg/mL) with the ABTS radical solution (absorbance = 0.700), the impact of ZnO NPs-FPNP on ABTS radical scavenging was ascertained. It was measured at 734 nm after the mixtures were left to sit for 6 min at room temperature in the dark [26].

Antibacterial activity of zinc oxide nanoparticles

Escherichia coli (ATCC 25922) and *Staphylococcus aureus* (ATCC 25923) were used to test how well the samples killed germs. The broth microdilution method was used in 96-well microplates for this work to find the minimum inhibitory concentration (MIC) and minimum bactericidal concentration (MBC). Bacterial inocula were generated from overnight cultures (24 h) on Mueller-Hinton Agar (MHA). Colonies were suspended in sterile saline solution and calibrated to the 0.5 McFarland standard (2×10^8 CFU/mL). More water was added to the suspension until the final bacterial concentration was approximately 5×10^5 CFU/mL. Test samples were subsequently made using Mueller-Hinton Broth (MHB) in two-fold repeated dilutions in the microplate wells, with each well infected with the bacterial suspension to get a total amount of 200 µL. Plates were kept warm at 35 ± 2 °C for a duration of 24 h. The MIC was established as the minimal concentration of the material that entirely prevented observable bacterial proliferation. To determine the MBC, 10 - 100 µL aliquots from wells exhibiting no growth were subcultured onto fresh MHA plates and incubated under identical conditions. The minimum concentration resulting in the absence of bacterial colony development was identified as the MBC. Antibacterial activity was designated as bactericidal when the MBC/MIC ratio was ≤4, and as bacteriostatic [27,28]

Statistical analysis

Three copies of each study were done, and the results were shown as the mean ± standard deviation (SD). GraphPad Prism version 9.0 (GraphPad Software, USA) and SPSS version 25.0 (IBM Corp., USA) were used for statistical studies. To look for changes in the antioxidant activity tests, a one-way analysis of variance (ANOVA) with Tukey's post hoc test was used. The IC_{50} values for radical scavenging activities were determined by nonlinear regression with a sigmoidal dose-response curve. Antibacterial assays produced MIC and MBC values from independent triplicate studies, with results provided as modal values corroborated by occurrence frequency across duplicates. A p - value below 0.05 was considered statistically significant. All biological assays, including antioxidant and antibacterial tests, were conducted independently in triplicate (n = 3), and data are expressed as mean ± standard deviation.

Results and discussion

Phytochemical analysis of extract

The phytochemical constituents of the FPNP, encompassing TPC and TFC, were effectively assessed utilising a UV-Vis spectrophotometer. The FPNP contains polyphenolic components at a concentration of 20.53 ± 1.20 mg GAE/g of sample. This discovery aligns with Nugroho *et al.* [29], who indicated that *N. fruticans* fruit peel comprises secondary metabolites, such as polyphenols [29]. In comparison to the report by Sudirman *et al.* [9], which demonstrated that *N. fruticans* fruit peel extracted with ethanol at concentrations of 50%, 60%, 70%, and 80% yielded polyphenolic contents between 8.08 and 16.63 mg GAE/g sample, the findings suggest that the polyphenolic content of the aqueous extract surpasses that of the ethanol extracts [9]. In a separate investigation conducted by Martin *et al*. [30], *N. fruticans* fruit peel extracted using hydroalcoholic solvents showed a polyphenolic concentration of 42.70 mg GAE/g sample [30]. The findings indicate that the polyphenolic concentration of an extract is determined not only by the solvent type but also by the plant material and the inherent qualities of the polyphenols. Ethanol-water mixtures are regarded as superior solvents for polyphenol extraction due to their ability to extract a broader spectrum of chemicals, including less polar components [31].

The FPNP was determined to contain flavonoid components at a concentration of 15.80 ± 1.46 mg QE/g of material. This outcome aligns with the observations of Fitri *et al.* [32], who documented the existence of flavonoids in the fruit peel of *N. fruticans* [32]. The current observation aligns with that of Moonrungsee *et al.* [33], where water extraction of *N. fruticans* fruit peel produced 16.34 mg QE/g of flavonoids [33]. Prasad *et al.* [34] showed a reduced flavonoid concentration of 3.6 mg rutin equivalent per gram of *N. fruticans* fruit peel [34]. The results collectively demonstrate that the aqueous extract of *N. fruticans* fruit peel possesses significant concentrations of polyphenols and flavonoids, thereby endorsing its potential use as a bioreductant in the environmentally sustainable synthesis of ZnO NPs, where these phytochemicals function as eco-friendly reducing and capping agents.

Figure 1 Zinc oxide nanoparticles generated using a biosynthesis process with a bioreductor of fruit peel extract of *N. fruticans* under a microwave-assisted approach.

Biosynthesis and characterization of zinc oxide nanoparticles

The natural formation of ZnO NPs utilising the FPNP via a microwave-assisted method was successfully accomplished. This technique achieved a recovery rate of 80.35%, with organoleptic qualities depicted in **Figure 1**. The biosynthesized ZnO NPs-FPNP were acquired as an amorphous yellowish-white powder devoid of any discernible odour. The natural formation of ZnO NPs using FPNP under microwave-assisted conditions is attributed to the synergistic roles of phytochemicals, alkaline environment, and microwave irradiation. The polyphenols and flavonoids present in FPNP act as natural reducing agents, facilitating the conversion of Zn^{2+} ions into ZnO nuclei, while simultaneously serving as capping agents that stabilize the growing nanoparticles through functional groups such as hydroxyl and carbonyl moieties [35]. The alkaline pH promotes the formation of $Zn(OH)_2$ intermediates, which subsequently dehydrate into ZnO [36]. Microwave irradiation provides rapid and uniform volumetric heating, accelerating nucleation and crystal growth while reducing reaction time and energy consumption. This synergistic process enables the successful green and natural formation of ZnO NPs without the use of toxic chemical reagents [37]. These traits align with those documented by Suresh *et al.* [38], who noted analogous qualities in ZnO NPs biosynthesised utilising *Cassia fistula* extract [38]. The ZnO NPs-FPNP synthesized under microwave-assisted conditions show advantageous physicochemical properties, as verified by spectrophotometric and associated analysis.

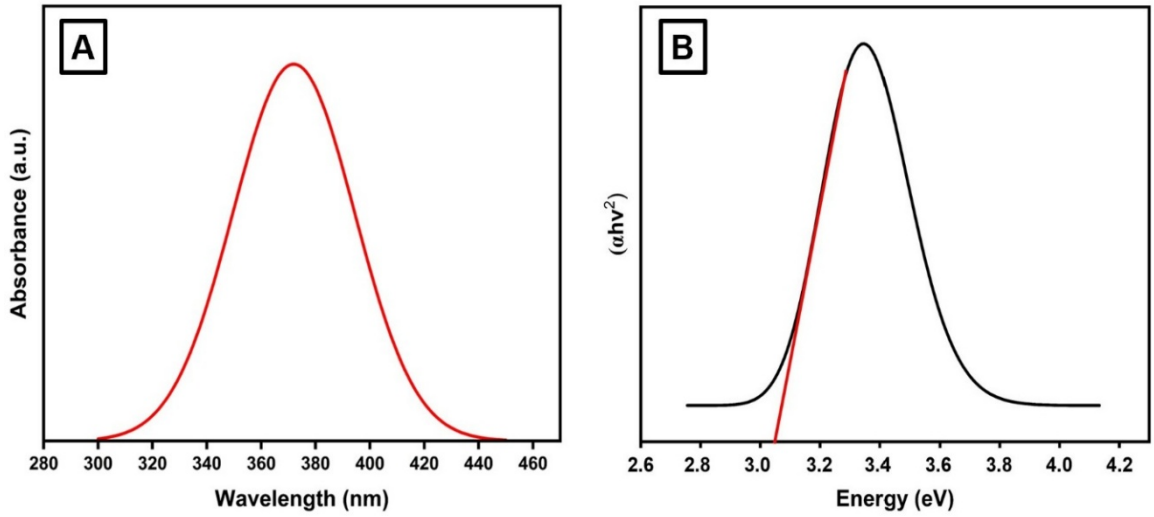

Figure 2 (A) UV-Visible absorption spectrum of ZnO NPs biosynthesized using *N. fruticans* fruit peel extract (ZnO NPs-FPNP), showing a characteristic absorption peak at approximately 370 nm, which confirms the successful formation of ZnO NPs. (B) Band gap energy analysis of ZnO NPs-FPNP derived from the absorption edge, indicating a band gap value of approximately 3.04 eV, consistent with nanoscale ZnO.

The UV-Vis spectrophotometric analysis, depicted in **Figure 2(A)**, revealed that the biosynthesized product consisted of ZnO NPs-FPNP, exhibiting a maximum absorption peak at 370 nm. The absorption peak at 370 nm corresponds to the characteristic band-to-band transition of ZnO NPs, confirming their successful formation. Such absorption in the ultraviolet region is typical for nanoscale ZnO and is influenced by particle size and surface interactions with phytochemicals present in the plant extract. This observation supports the findings of Mohd Yusof *et al.* [39], who identified a maximum peak at 360 nm [39]. The successful biosynthesis of ZnO NPs is often indicated by a peak absorption maximum in the range of 350 - 380 nm [40]. The band gap of ZnO NPs-FPNP was subsequently determined using the Tauc plot method, as illustrated in **Figure 2(B)**. The determined energy value of the ZnO NPs-FPNP in this investigation was 3.04 eV. This number signifies that the synthesised ZnO NPs-FPNP were pure and undoped. Prior studies have shown that various parameters, including the synthesis technique, particle size, and impurity content, influence the band gap energy of bio-synthesized ZnO NPs [41]. This aligns with the findings of Mohammadi *et al.* [42], who indicated that the band gap energy of ZnO NPs synthesized with *Punica granatum* fruit extract was inferior to that of chemically synthesized ZnO NPs [42]. Plant extracts have been reported to induce plasmon-like optical effects in ZnO NPs through surface defect formation and modification of the local dielectric environment, therefore decreasing the energy necessary for electronic transitions. Consequently, a diminished band gap energy may augment the medicinal efficacy of ZnO NPs [42].

Furthermore, to facilitate the effective production of ZnO NPs-FPNP under microwave-assisted conditions, the ZnO NPs-FPNP were characterised via FTIR, as illustrated in **Figure 3**. The FTIR spectra of the ZnO NPs-FPNP exhibited a pronounced absorption band at 3,490 cm^{-1}. This absorption band corresponds to the OH stretching vibration from polyphenolic chemicals in the extract, indicating that chemical interactions between the extract and the ZnO precursor occurred during nanoparticle production. Jaishi *et al.* [43] reported analogous findings, noting a pronounced OH absorption at 3,317 cm^{-1} in their synthesized ZnO NPs [43] Similarly, Jayachandran *et al*. [44] detected OH absorption linked to polyphenols at 3,275 cm^{-1} in ZnO NPs [44]. The presence of OH absorption bands in the FTIR spectrum is a definitive property of biosynthesized ZnO NPs mediated by plant extracts [45]. The OH absorption band observed in the FTIR spectrum originates from hydroxyl-containing phytochemicals adsorbed on the ZnO surface, which function as natural capping agents during biosynthesis. Surface hydroxylation resulting from aqueous synthesis

conditions further supports the green-mediated formation of ZnO NPs [46]. Meanwhile, the FTIR spectra displayed pronounced absorption bands at 2,310, 1,620, and 1,433 cm^{-1}, indicative of the C–H, C=C, and C=O stretching vibrations of alkanes and ketones. Selim *et al*. [47] indicate that these absorptions signify the main and secondary phytochemicals found in the extract used for synthesis [47]. Khan *et al*. [48] further substantiated this observation, indicating that ZnO NPs synthesized from strawberry waste had analogous absorption bands at 2,345, 1,629, and 1,418 cm^{-1}, respectively [48] The successful biogenesis of ZnO NPs, as demonstrated by the FTIR data, was indicated by absorption bands at 982 and 497 cm^{-1}. The band at 982 cm^{-1} indicates C–O stretching, signifying the interaction between the extract and ZnO, whereas the band at 497 cm^{-1} denotes the characteristic stretching vibration of pure ZnO. This observation aligns with the findings of Thi *et al*. [49], who documented a ZnO vibration at 495 cm^{-1} [49].

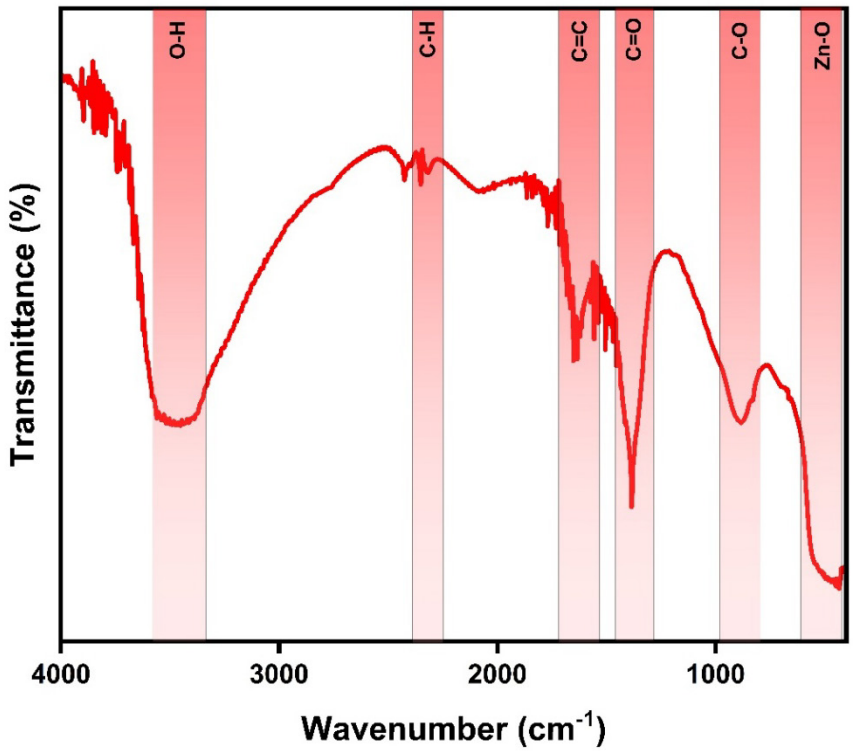

Figure 3 FTIR spectrum of ZnO NPs biosynthesized using *N. fruticans* fruit peel extract (ZnO NPs-FPNP), showing characteristic vibrational bands corresponding to surface-bound phytochemical functional groups. The absorption bands observed at various wavenumbers (cm^{-1}), including broad O–H stretching, C=O/C–O vibrations, and Zn–O stretching in the low wavenumber region, confirm the involvement of plant-derived biomolecules in nanoparticle formation and stabilization.

Additionally, the attributes of ZnO NPs-FPNPS identified in this work include particle size, polydispersity index, and zeta potential, as illustrated in **Figure 4**. According to **Figure 4(A)**, the mean particle size of ZnO NPs-FPNP in this work is 234 ± 59.5 nm. This indicates that the resultant particles remain quite large, as they exceed 100 nm. The larger particle size obtained from PSA analysis reflects hydrodynamic diameter and partial aggregation of ZnO NPs, while TEM analysis confirms the presence of primary nanoparticles within the nanoscale range [50]. Numerous studies have indicated comparable particle sizes, including the findings of Rusli *et al.* [51], which revealed that ZnO NPs derived from *Garcinia mangosta* extract exhibited an average particle size of 641.97 nm [51]. A further investigation by Hussien *et al.* [52] indicated that the synthesized ZnO NPs exhibited a particle size of 249.8 nm [52]. Nonetheless, alternative research, including the one by Faisal *et al.* [53], effectively synthesised ZnO NPs with a particle size of

66 nm [53]. The PI obtained in this investigation was 0.516. This number signifies that the ZnO NPs produced exhibit a somewhat broad distribution. The relatively high polydispersity index indicates a broad particle size distribution, which is a common feature of plant extract-mediated green synthesis due to heterogeneous nucleation and biomolecule-induced aggregation. Such polydispersity may influence size-dependent properties, dispersion stability, and interaction consistency in certain applications [54]. Nonetheless, this is acceptable as the phytochemical substances present in the extract typically lead to an elevation in PI. Likewise, Ibrahim *et al.* [55]. indicated that ZnO NPs synthesized with *Azadirachta indica* extract had a substantial PI of 0.472 [55]. Mishra *et al.* [56] found that ZnO NPs synthesized with *Trichoderma harzianum* had a greater PI of 1 [56]. The zeta potential energy of the ZnO NPs synthesized in this study was assessed to ensure their stability, as illustrated in **Figure 4(B)**. The ZnO NPs in this investigation exhibited a zeta potential of –25.7 ± 1.50 mV. The results indicate that the synthesized ZnO NPs exhibit adequate electrostatic stability due to the negatively charged groups derived from the *N. fruticans* fruit peel extract. The results obtained are not substantially different from those published by Jain *et al*. [57] at -30 mV [57]. Hamrayev *et al.* [58] reported a zeta potential energy of +23.19 mV [58]. A zeta potential energy of 20 - 30 mV signifies that the ZnO NPs exhibit considerable stability [58]. This results from the robust electrostatic forces among particles, which inhibit the aggregation of the dispersion, although minor clusters may nevertheless occasionally develop. Although electrostatic repulsion stabilizes the dispersion, occasional nanoparticle collisions and biomolecule-mediated interactions may result in the formation of minor clusters without causing significant aggregation or sedimentation [59].

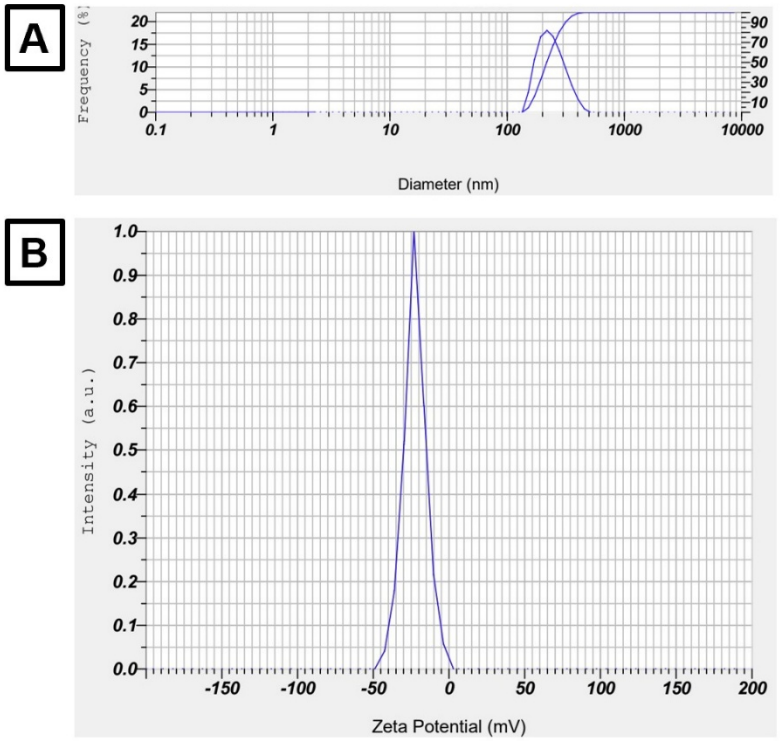

Figure 4 (A) Particle size distribution and polydispersity index (PDI) of ZnO NPs biosynthesized using *N. fruticans* fruit peel extract (ZnO NPs-FPNP) under microwave-assisted conditions, showing a relatively broad hydrodynamic size distribution. (B) Zeta potential of ZnO NPs-FPNP, indicating a negatively charged surface that contributes to colloidal stability and reduced aggregation in aqueous dispersion.

The surface and elements of ZnO NPs-FPNP were analyzed by SEM, TEM, and EDX to corroborate the properties of PSA and ZPA, as illustrated in **Figure 5**. **Figure 5(A)** demonstrates that the resultant ZnO NPs-

FPNP exhibit an uneven shape, with a fundamental particle size at the nanometre scale, which tends to agglomerate into micrometer clusters. This aggregation frequently arises in the production of plant extracts due to the presence of organic molecules that function as stabilisers. Therefore, the irregular morphology reflects heterogeneous nucleation and anisotropic growth during green synthesis, while plant-derived biomolecules effectively restrict particle growth, preserving nanoscale dimensions [60]. This aligns with the PI values acquired and documented in this investigation. This outcome is not inherently unfavourable. An earlier study by Alprol *et al.* [61] showed that the agglomeration of ZnO NPs can augment the material's surface area, thus improving its biological activity [61]. Mahajan *et al.* [62] corroborate this, revealing that inside agglomerates, smaller particles induce a twofold nucleation mechanism, thereby providing multiple reactive sites [62]. The study proceeded with TEM to obtain a clearer structure of the resultant ZnO NPs, as illustrated in **Figure 5(B)**. TEM research revealed that ZnO NPs had a predominant rod-like morphology, measuring approximately 50 - 150 nm in length and 20 - 40 nm in diameter. Certain particles appeared to agglomerate, yet individual particles were distinctly identifiable. Zhou *et al*. [63] indicated that rod-shaped ZnO NPs are equivalent to wurtzite crystal ZnO nanoparticles [63]. This morphology is indicative of the biosynthesis technique utilising extracts via a microwave approach, as documented by Bharathi *et al.* [64]. Subsequently, to verify the successful production of ZnO NPs utilising *N. fruticans* fruit peel extract via the microwave method, the presence of zinc and oxygen was assessed using energy-dispersive X-ray spectroscopy (EDX). **Figure 5(C)** demonstrates that the resultant chemical comprises three elements: zinc, oxygen, and carbon. The presence of zinc verifies that the primary component of the nanoparticles is included in the resultant product. The presence of oxygen signifies the formation of ZnO in conjunction with Zn. The existence of oxygen facilitates the creation of Zn-O bonds, as corroborated by FTIR data. The presence of carbon likely derives from organic chemicals in the extract, suggesting a distinctive aspect of the green synthesis process.

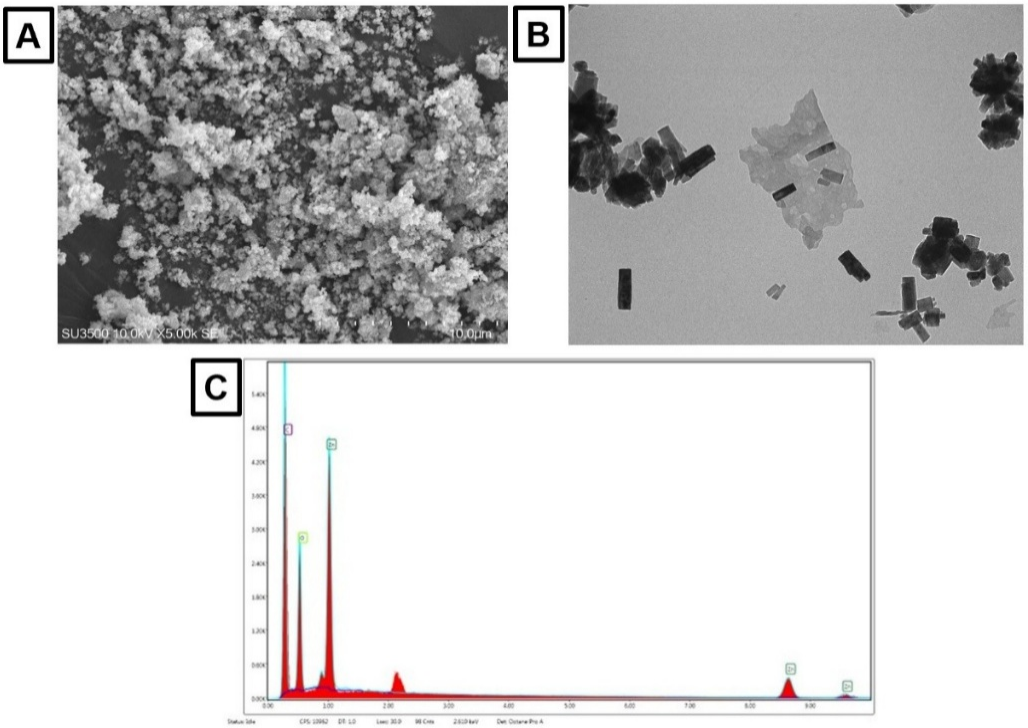

Figure 5 (A) SEM micrograph of ZnO NPs biosynthesized via green synthesis using *N. fruticans* fruit peel extract, showing aggregated particles with irregular morphology. (B) TEM micrograph revealing the fundamental particle size of ZnO NPs within the nanometre scale. (C) EDX spectrum confirming the elemental composition of the biosynthesized ZnO NPs, with predominant signals corresponding to zinc (Zn) and oxygen (O), indicating high purity of the synthesized material.

The TEM results indicate that the generated ZnO NPs-FPNP are rod-shaped, aligning with the wurtzite crystal structure. The identification of ZnO NPs via XRD, as illustrated in **Figure 6(A)**, corroborated this. The principal intensity peaks identified at 2θ were 31.7° (100), 34.4° (002), 36.2° (101), 47.5° (102), 56.6° (110), 62.8° (103), 66.3° (200), and 68.0° (112). The observed XRD diffraction peaks correspond to the characteristic lattice planes of hexagonal wurtzite ZnO, which is the most thermodynamically stable crystal structure of ZnO under ambient conditions. The diffraction peaks indexed to the (100), (002), (101), (102), (110), (103), (200), and (112) planes match well with the standard JCPDS card No. 36 - 1451, confirming the formation of phase-pure ZnO with a hexagonal wurtzite structure. Moreover, our findings align with those presented by Ashaduzzaman *et al.* [10], who discovered that biosynthesised ZnO NPs utilising the microwave method display peaks at 2θ intensities of 31.86°, 34.55°, 36.36°, 47.65°, 56.68°, 62.85°, 66.39°, 68.09°, and 69.18° [10]. The crystal structure of ZnO NPs significantly influences their stability and biological efficacy, particularly in terms of antibacterial properties [10]. According to Silva *et al.* [65], variations in crystal morphology lead to alterations in H^+/OH^- ion adsorption and Zn^{2+} solubility, both of which influence reactive oxygen species (ROS) generation to suppress microbial proliferation [65]. Subsequently, to evaluate the stability of the synthesized ZnO NPs-FPNP, thermal examination via Differential Thermogravimetry (DTG) was conducted, as illustrated in **Figure 6(B)**. The thermal analysis results indicated that the ZnO NPs-FPNP underwent phase transitions at elevated temperatures, specifically exhibiting peaks at temperatures below 100 °C and over 150 °C. During the early phase, mass loss transpires as a result of the evaporation of free and adsorbed water from the nanoparticle surface. In the second phase, there was no notable mass loss up to 800 °C, demonstrating that the ZnO structure was thermally stable and did not experience additional disintegration. This aligns with the findings of Demissie *et al.* [66], which indicated that ZnO NPs synthesised with *Lippia adoensis* extract maintained stability despite temperatures above 400 °C [66]. In alignment with Abomuti *et al*. [67], revealed that the organic chemicals in *Salvia officinalis* extract may safeguard ZnO NPs from degradation at temperatures exceeding 400 °C [67]. The features of ZnO NPs synthesised utilising *N. fruticans* fruit peel extract using the microwave method demonstrate commendable quality in both chemical and physical aspects, hence endorsing further investigation in the biomedical domain.

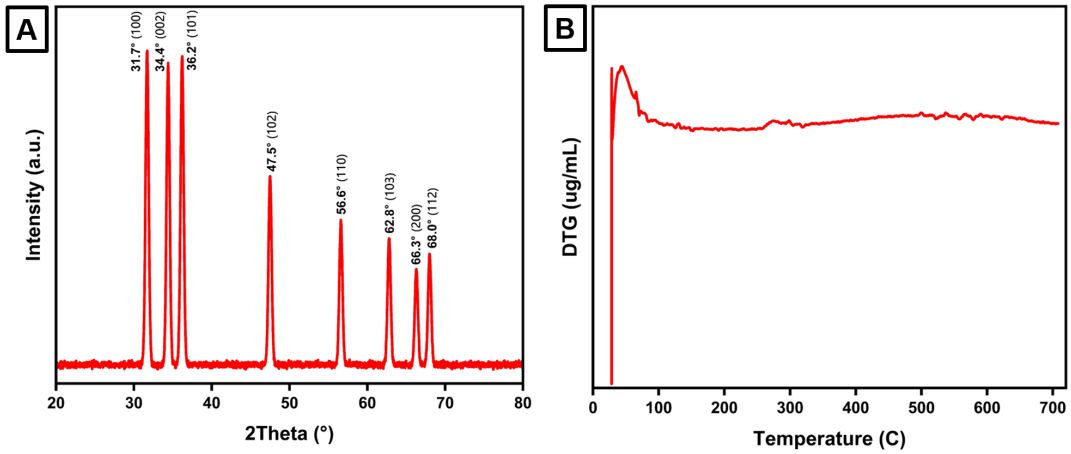

Figure 6 (A) XRD pattern of ZnO NPs biosynthesized via green synthesis using *N. fruticans* fruit peel extract, showing diffraction peaks corresponding to the hexagonal wurtzite crystal structure of ZnO, confirming phase purity and good crystallinity. (B) Thermal stability profile of the biosynthesized ZnO NPs obtained from thermogravimetric analysis, indicating weight loss associated with the removal of surface-bound phytochemicals and thermal stability of the ZnO framework at higher temperatures.

Antioxidant activity of zinc oxide nanoparticles

This study assessed the antioxidant activity of FPNP and ZnO NPs-FPNP by a microwave method, utilising DPPH and ABTS radical scavenging assays, as illustrated in **Figure 7**. **Figure 7(A)** illustrates that the DPPH radical scavenging activity of each test group escalated with rising doses from 31.25 to 500 µg/mL ($p < 0.0001$). At the minimal concentration, ascorbic acid (AA) exhibited the greatest inhibitory action at 53.43 ± 0.83%, followed by ZnO NPs-FPNP at 32.15 ± 1.46%, and FPNP at 11.37 ± 0.94%. The values remained statistically significant with $p < 0.05$. Notably, at the maximum concentration, while AA exhibited the highest percentage inhibition of DPPH radical scavenging at 91.41 ± 1.05%, this result was not statistically distinct from the DPPH radical inhibition percentage by ZnO NPs-FPNP at 500 µg/mL, which was 87.22 ± 3.21% ($p > 0.05$). At a dose of 500 µg/mL, FPNP demonstrated a 52.08 ± 1.81% increase in the inhibition of DPPH radicals, but this result remained statistically different from the other two groups ($p < 0.05$). Ultimately, ZnO NPs-FPNP showed efficacy equivalent to that of AA in suppressing DPPH radicals at a dose of 500 µg/mL. The impact of ZnO NPs-FPNP injection on the inhibition of ABTS radicals is illustrated in **Figure 7(B)**. The impact of ABTS radical inhibition across all test groups was statistically significant and correlated with increased concentration ($p < 0.001$). In **Figure 7(B)**, it was shown that AA exhibited no significant difference in its ability to suppress ABTS radicals with ZnO NPs-FPNP throughout concentrations ranging from 31.25 to 500 µg/mL, with $p > 0.05$. Simultaneously, FPNP exhibited a statistically significant difference in the inhibition of ABTS radicals compared to the other 2 groups at each test concentration, with p values less than 0.05, respectively. At the minimal dose, the greatest DPPH radical inhibition percentage was achieved with AA administration at 36.47 ± 0.94%, succeeded by ZnO NPs-FPNP at 33.49 ± 1.06%, and FPNP at 13.52 ± 1.05%. A comparable outcome was observed at the maximum concentration of 500 µg/mL for each group, suppressing ABTS radicals by 85.41 ± 1.03%, 83.74 ± 1.69%, and 57.26 ± 1.52%, respectively. The biosynthesis of ZnO NPs-FPNP effectively enhanced the DPPH and ABTS radical inhibition efficacy compared to FPNP described by the inhibitory concentration 50 (IC_{50}) in **Table 1**. The IC_{50} of ZnO NPs-FPNP to inhibit DPPH and ABTS were 53.64 ± 2.70 µg/mL and 56.57 ± 2.23 µg/mL, respectively. It is illustrated more strongly significant of FPNP to inhibit DPPH and ABTS, was 465.68 ± 5.71 µg/mL and 361.35 ± 5.03 µg/mL, respectively. Unfortunately, it is still observed lowest than ascorbic acid, was 10.68 ± 0.84 µg/mL and 9.77 ± 0.51 µg/mL, respectively. However, it indicates its potential as a competitive antioxidant agent.

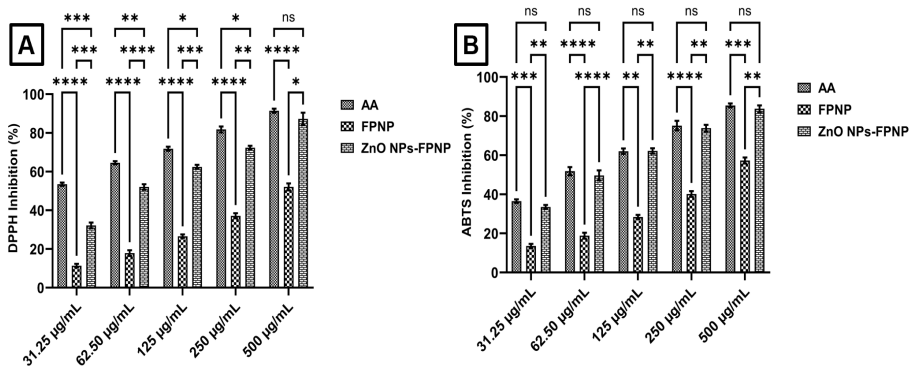

Figure 7 (A) DPPH radical inhibition, (B) ABTS radical inhibition by ZnO NPs under green synthesis. AA is defined as ascorbic acid, FPNP is defined as fruit peel extract of *Nypa fruticans*, and ZnO NPs-FPNP is defined as zinc oxide nanoparticles synthesized using fruit peel extract of *N. fruticans* with microwave-assisted. **** is defined as the group significantly different with $p < 0.0001$, *** is defined as the group significantly different with $p < 0.001$, ** is defined as the group significantly different with $p < 0.01$, * is defined as the group significantly different with $p < 0.05$, and ^{ns} is defined as the group not significantly different with $p > 0.05$.

Table 1 Inhibitory concentration 50 (IC_{50}) of sample tests to inhibit DPPH and ABTS radical.

Sample	IC_{50} (µg/mL)	
	DPPH	**ABTS**
FPNP	465.68 ± 5.71	361.35 ± 5.03
ZnONPs-FPNP	53.64 ± 2.70	56.57 ± 2.23
Ascorbic acid	10.68 ± 0.84	9.77 ± 0.51

FPNP: Fruti peel extract of *Nypa fruticans*, ZnONPs-FPNP: Zinc oxide nanoparticles synthesized using *Nypa fruticans* fruit peel extract.

Investigations on the antioxidant properties of ZnO NPs are not new to the literature. Azizi *et al*. [68] documented that biosynthesized ZnO NPs derived from *Citrullus colocynthis* by a microwave method reduced DPPH radicals by 75% at a concentration of 1 g/mL [68]. Nagajyothi *et al.* [69] observed that ZnO NPs synthesised with *Polygala tenuifolia* root extract inhibited DPPH radicals by 45% at a concentration of 1 mg/mL [69]. Meanwhile, Albarakaty *et al*. [22] indicated that ZnO NPs synthesised using *Moringa oleifera* extract may suppress DPPH radicals by as much as 90% at a dosage of 100 mg/mL [22]. In this investigation, approximately 300 µg/mL was required to inhibit each DPPH and ABTS radical by 75%, while around 60 µg/mL was sufficient to achieve a 50% inhibition of each radical. Consequently, ZnO nanoparticles synthesised from *N. fruticans* fruit peel extract by a microwave method exhibit significant potential as antioxidant agents. The factors influencing the antioxidant activity of ZnO NPs are intriguing [70]. ZnO NPs can release Zn^{2+} ions, which participate in redox reactions by sequestering free electrons from radicals, so stabilising them [71]. Moreover, due to the structural structure of ZnO NPs, which possesses several oxygen vacancies acting as electron donors, they may rapidly neutralize free radicals [72]. Moreover, ZnO NPs possess a semiconductor band gap, enabling the generation of free electrons and holes upon excitation [73]. The liberated electrons interact with DPPH or ABTS radicals, neutralising them [73]. There are important distinctions between the antioxidant processes of ZnO NPs and those of organic antioxidants such as ascorbic acid. Nonetheless, the outcome remains unchanged, specifically a reduction in the concentration of free radicals.

Antibacterial activity of zinc oxide nanoparticles

This work presents the antibacterial efficacy of ZnO NPs-FPNP against *E. coli* and *S. aureus*, determined by the minimum inhibitory concentration (MIC) and minimum bactericidal concentration (MBC) within a concentration range of 0.5 to 1024 µg/mL. According to the findings presented in **Table 2**, FPNP effectively inhibited the proliferation of *E. coli* and *S. aureus* at doses of 512 and 256 µg/mL, respectively. ZnO NPs-FPNP effectively inhibited the growth of *E. coli* and *S. aureus* at lower doses than FPNP, specifically 64 and 32 µg/mL, respectively. Gentamicin effectively inhibited the growth of *E. coli* and *S. aureus* at doses of 1 and 0.5 µg/mL, respectively. Statistical analysis indicates significant differences among each test group with $p < 0.05$. Additionally, each test group was reported to effectively eliminate *E. coli* and *S. aureus* at specific amounts. FPNP has been found to eradicate *E. coli* and *S. aureus* at a dose of 1024 µg/mL. Conversely, ZnO NPs-FPNP necessitated minimal dosages to eradicate *E. coli* and *S. aureus*, specifically 128 and 64 µg/mL, respectively. Gentamicin effectively eradicated *E. coli* and *S. aureus* at concentrations of 2 and 1 µg/mL, respectively. Statistically, a significant difference was seen among all test groups in the eradication of *E. coli* and *S. aureus*, with $p < 0.05$. Nonetheless, FPNP and ZnO NPs-FPNP are classified as possessing a bactericidal action due to the MBC/MIC ratio exceeding 1.

Table 2 Antibacterial activity of ZnO NPs-FPNP against *E. coli* and *S. aureus.*

Sample	Strain	MIC (mean, µg/mL)	MBC (µg/mL)	MBC/MIC ratio	Interpretation
FPNP	*E. coli* ATCC 25922	512[a]	1024[a]	2	Bactericidal
	S. aureus ATCC 25923	256[d]	1024[d]	4	Bactericidal
ZnO NPs-FPNP	*E. coli* ATCC 25922	64[b]	128[b]	2	Bactericidal
	S. aureus ATCC 25923	32[e]	64[e]	2	Bactericidal
Gentamicin	*E. coli* ATCC 25922	1[c]	2[c]	2	Bactericidal
	S. aureus ATCC 25923	0.5[f]	1[f]	2	Bactericidal
Solvent control	*E. coli* ATCC 25922	-	-	-	Not active
	S. aureus ATCC 25923	-	-	-	Not active

FPNP (fruit peel extract of *N. fruticans*), ZnO NPs-FPNP (zinc oxide nanoparticles synthesized using FPNP), MIC (minimum inhibitory concentration), MBC (minimum bactericidal concentration), and different letter is defined as significantly different with $p < 0.05$.

This study indicates that FPNP exhibits moderate antibacterial action, whereas ZnO NPs-FPNP demonstrates significantly greater activity; however, gentamicin remains the most effective agent against *E. coli* and *S. aureus*. This study demonstrates that employing FPNP in the microwave-assisted biosynthesis of ZnO NPs can enhance antibacterial efficacy by 8 to 16 times relative to FPNP alone. Furthermore, this signifies that alterations in particle structure or morphology influence their biological activity. Goyal *et al*. [74] corroborate this, revealing that variations in the shape of ZnO NPs synthesised using chemical techniques influence their antibacterial efficacy differently [74]. Furthermore, Happy *et al*. [75] indicated that ZnO NPs synthesised from *Cassia alata* effectively inhibited the development of *E. coli* at an IC_{50} of 20 µg/mL [75]. A study conducted by Irfan *et al*. [76] demonstrated that ZnO NPs synthesised from *Moringa oleifera* effectively inhibited the development of *E. coli* and *S. aureus*, with maximum inhibition zones of 22 and 21 mm, respectively [76]. These investigations validate that ZnO NPs produced via green synthesis possess potential as antibacterial agents, particularly against *E. coli* and *S. aureus*. This raises the intriguing topic of the mechanism by which ZnO NPs function as antibacterial agents. Obeizi *et al*. [77] indicated that ZnO NPs biosynthesised from the essential oil of *Eucalyptus globulus* effectively inhibited the growth of *S. aureus* by up to 85% through biofilm suppression [77]. Abdelghafar *et al.* [78] demonstrated that ZnO NPs can prevent biofilm formation by up to 50% against *S. aureus* [78]. The antibiofilm impact is further supported by evidence indicating that ZnO NPs can enhance the generation of reactive oxygen species (ROS), including superoxide anions, hydroxyl radicals, and hydrogen peroxide, which adversely affect bacterial cells [79]. ZnO NPs are documented to aggregate on the external surface of bacterial cells [80]. The adequate concentration of Zn^{2+} ions induces the degradation of the bacterial cell membrane and obstructs amyloid peptide fibrillation, thereby averting biofilm formation and commencing bacterial mortality [81]. The findings indicate that ZnO NPs production utilising *N. fruticans* fruit peel via the microwave method effectively inhibits bacterial growth and holds promise for development as an antibacterial agent.

Conclusions

The green synthesis of ZnO NPs utilising *N. fruticans* fruit peel with microwave assistance offers an environmentally benign, quick, straightforward, non-toxic, and effective method for nanoparticle production. The phytochemical composition of fruit peel extract from *N. fruticans* was determined using Folin-Ciocalteau and aluminium chloride tests. Concurrently, synthesised ZnO NPs-FPNP were characterised using UV-Vis absorption spectroscopy, FTIR, PSA, ZPA, SEM, TEM, EDX, XRD, and DTG. The fruit peel extract of *N. fruticans* contains total phenolic and flavonoid of 20.53 ± 1.20 mg GAE/g and 15.80 ± 1.46 mg QE/g of sample, respectively. Consequently, the biosynthesised ZnO NPs were obtained as an amorphous yellowish-white powder, lacking any detectable odour, and were thoroughly characterised. The visible spectra indicated a prominent peak at 370 nm, corresponding to a band gap energy of 3.04 eV, thus validating the production of the nanoparticles. FTIR spectra showed that the peak at 497 cm^{-1} corresponds to the stretching vibration of Zn-O, which is the definitive peak for the creation of ZnO NPs. The particle size of ZnO NPs, as indicated by PSA, is 234 ± 59.5 nm, with a polydispersity index of 0.516. The zeta potential energy of ZnO NPs was found to be –25.7 ± 1.50 mV, indicating the stability of the ZnO NPs. The SEM micrograph revealed an irregular morphology, with primary particle dimensions at the nanometre scale, which tend to aggregate into micrometre clusters. TEM research indicated that ZnO NPs had a mostly rod-like shape, with lengths ranging from around 50 to 150 nm and diameters between 20 and 40 nm. The ZnO NPs were proven to contain three elements: Zinc, oxygen, and carbon. The XRD pattern verified that the ZnO NPs possess a wurtzite crystal structure exhibiting remarkable stability at temperatures exceeding 400 °C. Despite the promising antioxidant and antibacterial performance of the biosynthesized ZnO NPs, it is important to acknowledge certain physicochemical limitations of the current formulation. The relatively large hydrodynamic particle size observed in PSA analysis, mainly attributed to partial aggregation and phytochemical capping layers, may influence nanoparticle mobility and biological interactions. Nevertheless, the observed biological activities indicate that surface chemistry and electronic properties play a more decisive role than particle size alone. Future optimization of synthesis parameters and dispersion conditions is expected to improve particle size uniformity while further enhancing biological performance.

Acknowledgements

This study was financially supported by Direktorat Penelitian dan Pengabdian Kepada Masyarakat (DPPM), Indonesia (No: 47/SPK/LL1/AL.04.03/PL/2025).

Declaration of Generative AI in Scientific Writing

During the preparation of this study, the authors used ChatGPT in order to verify the grammar and improve the readability. After using this tool/service, the authors reviewed and edited the content as needed and take full responsibility for the content of the article.

CRediT Author Statement

Rezza Destri Anggi: Conceptualization, methodology, software, investigation, project administration, writing-original draft. **Diding Pradita:** Writing-original draft, investigation, visualization, project administration. **Adek Chan:** Writing – original draft, investigation, validation. **Hanafis Sastra Winata:** Writing-review and editing, methodology, and formal analysis. **Mutiara Qisthina Hanif:** Writing-original draft, formal analysis, project administration. **Muhammad Fauzan Lubis:** Conceptualization, investigation, supervision, writing-review and editing.

References

[1] AW Digisu, AB Yaebyo, WL Kebede, DY Kebede and DK Molla. Biogenic synthesis, optimization, and characterization of zinc oxide nanoparticles using *Rumex abyssinicus Jacq* root extract for antioxidant and antibacterial activities. *Results in Chemistry* 2024; **12**, 101857.

[2] KV Dhandapani, D Anbumani, AD Gandhi, P Annamalai, BS Muthuvenkatachalam, P Kavitha and B Ranganathan. Green route for the synthesis of zinc oxide nanoparticles from *Melia azedarach* leaf extract and evaluation of their antioxidant and antibacterial activities. *Biocatalysis and Agricultural Biotechnology* 2020; **24**, 101517.

[3] H Chandra, D Patel, P Kumari, JS Jangwan and S Yadav. Phyto-mediated synthesis of zinc oxide nanoparticles of *Berberis aristata*: Characterization, antioxidant activity and antibacterial activity with special reference to urinary tract pathogens. *Materials Science and Engineering: C* 2019; **102**, 212-220.

[4] S Dey, D lochan Mohanty, N Divya, V Bakshi, A Mohanty, D Rath, S Das, A Mondal, S Roy and R Sabui. A critical review on zinc oxide nanoparticles: Synthesis, properties and biomedical applications. *Intelligent Pharmacy* 2025; **3(1)**, 53-70.

[5] Jayalekshmi C, R Periakaruppan, V Romanovski, KSVSelvaraj and N Al-Dayan. Calotropis gigantea latex-derived zinc oxide nanoparticles: Biosynthesis, characterization, and biofunctional applications. *Eng* 2024; **5(3)**, 1399-1406.

[6] AK Khajuria, A Kandwal, RK Sharma, RK Bachheti, LA Worku and A Bachheti. *In vitro* antioxidant and antibacterial activities of biogenic synthesized zinc oxide nanoparticles using leaf extract of *Mallotus philippinensis* Mull. Arg. *Scientific Reports* 2025; **15**, 6541.

[7] MM Abisha, D Usha, BM Ashwin, A Yardily and MS Dennison. Microwave-assisted green synthesized ZnO nanoparticles: An experimental and computational investigation. *Discover Applied Sciences* 2025; **7**, 177.

[8] MS Kang and KY Hyun. Antinociceptive and anti-inflammatory effects of *Nypa fruticans* wurmb by suppressing TRPV1 in the sciatic neuropathies. *Nutrients* 2020; **12(1)**, 135.

[9] S Sudirman, AK Wardana, Herpandi, I Widiastuti, DI Sari and M Janna. Antioxidant activity of polyphenol compounds extracted from *Nypa fruticans* Wurmb. (Nipa palm) fruit husk with different ethanol concentration. *International Journal of Secondary Metabolite* 2024; **11(2)**, 355-363.

[10] M Ashaduzzaman, MAA Muhit, SC Dey, MM Rahaman, HNM Hasan, N Mustary, MK Hossain and MK Das. Microwave assisted starch stabilized green synthesis of zinc oxide nanoparticles for antibacterial and photocatalytic applications. *Scientific Reports* 2025; **15**, 28288.

[11] M Hasanpoor, M Aliofkhazraei and H Delavari. Microwave-assisted synthesis of zinc oxide nanoparticles. *Procedia Materials Science* 2015; **11**, 320-325.

[12] Y Hao, Y Wang, L Zhang, F Liu, Y Jin, J Long, S Chen, G Duan and H Yang. Advances in antibacterial activity of zinc oxide nanoparticles against *Staphylococcus aureus* (Review). *Biomedical Reports* 2024; **21(5)**, 161.

[13] C Mallikarjunaswamy, VL Ranganatha, R Ramu, Udayabhanu and G Nagaraju. Facile microwave-assisted green synthesis of ZnO nanoparticles: Application to photodegradation, antibacterial and antioxidant. *Journal of Materials Science: Materials in Electronics* 2020; **31**, 1004-1021.

[14] CA Acar, MA Gencer, S Pehlivanoglu, S Yesilot and S Donmez. Green and eco-friendly biosynthesis of zinc oxide nanoparticles using *Calendula officinalis* flower extract: Wound healing potential and antioxidant activity. *International Wound Journal* 2023; **21(1)**, 14413.

[15] H Jan, M Shah, H Usman, MA Khan, M Zia, C Hano and BH Abbasi. Biogenic synthesis and characterization of antimicrobial and antiparasitic zinc oxide (ZnO) nanoparticles using aqueous extracts of the himalayan columbine (*Aquilegia pubiflora*). *Frontiers in Materials* 2020; **7**, 00249.

[16] S Sumaiyah, R Murwanti, DN Illian, MF Lubis and K Tampubolon. New insights of response surface methodology approach in optimizing total phenolic content of *Zanthoxylum acanthopodium* DC. fruit extracted using microwave-assisted extraction and the impact to antioxidant activity. *Indonesian Journal of Chemistry* 2024; **24(6)**, 1743-1759.

[17] MF Lubis, PAZ Hasibuan, H Syahputra, JM Keliat, VE Kaban and R Astyka. Duku (Lansium domesticum) leaves extract induces cell cycle arrest and apoptosis of HepG2 cells via PI3K/Akt pathways. *Trends in Sciences* 2023; **20(2)**, 6437.

[18] IE Doicin, MD Preda, IA Neacsu, VL Ene, AC Birca, BS Vasile and E Andronescu. Tailoring zinc oxide nanoparticles via microwave-assisted hydrothermal synthesis for enhanced antibacterial properties. *Applied Sciences* 2024; **14(17)**, 7854.

[19] PK Jha, T Jaidumrong, D Rokaya and C Ovatlarnporn. *Callistemon viminalis* leaf extract

phytochemicals modified silver-ruthenium bimetallic zinc oxide nanocomposite biosynthesis: Application on nanocoating photocatalytic *Escherichia coli* disinfection. RSC Advances 2024; **14(16)**, 11017-11026.

[20] P Basnet, PK Jha, A Gupta and S Chatterjee. Synergistic effect of tea-phytochemicals, noble metals and zno nano-photo-composites for combating resistance of bacterial growth. *Journal of Nano Research* 2021; **70**, 53-66.

[21] RD Wouters, PCL Muraro, DM Druzian, AR Viana, E de Oliveira Pinto, JKL da Silva, BS Vizzotto, YPM Ruiz, A Galembeck, G Pavoski, DCR Espinosa and WL da Silva. Zinc oxide nanoparticles: Biosynthesis, characterization, biological activity and photocatalytic degradation for tartrazine yellow dye. *Journal of Molecular Liquids* 2023; **371**, 121090.

[22] FMA Albarakaty, MI Alzaban, N Alharbi, FS Bagrwan, ARM Abd El-Aziz and MA Mahmoud. Zinc oxide nanoparticles, biosynthesis, characterization and their potent photocatalytic degradation, and antioxidant activities. *Journal of King Saud University - Science* 2022; **35(1)**, 102434.

[23] MS Jamal, MS Chowdhury, S Bajgai, M Hossain, A Laref, PK Jha and K Techato. Comparative studies on the morphological, structural and optical properties of NiO thin films grown by vacuum and non-vacuum deposition techniques. *Materials Research Express* 2021; **8**, 126404.

[24] PK Jha, C Chawengkijwanich, C Pokum, P Soison and K Techato. Antibacterial activities of biosynthesized zinc oxide nanoparticles and silver-zinc oxide nanocomposites using camellia sinensis leaf extract. *Trends in Sciences* 2023; **20(3)**, 5649.

[25] PK Jha, C Chawengkijwanich, K Techato, W Limbut and M Luengchavanon. Callistemon viminalis leaf extract mediated biosynthesis of Ag, rGO-Ag-ZnO nanomaterials for catalytic PEM fuel cell application. *Trends in Sciences* 2022; **19(11)**, 493.

[26] LD Lubis, AT Prananda, NA Juwita, MA Nasution, RA Syahputra, S Sumaiyah, RR Lubis, MF Lubis, R Astyka and JF Atiqah. Unveiling antioxidant capacity of standardized chitosan-tripolyphosphate microcapsules containing polyphenol-rich extract of *Portulaca oleraceae*. *Heliyon* 2024; **10(8)**, 29541.

[27] A Klančnik, S Piskernik, B Jeršek and SS Možina. Evaluation of diffusion and dilution methods to determine the antibacterial activity of plant extracts. *Journal of Microbiological Methods* 2010; **81(2)**, 121-126.

[28] G Adwan, B Abu-Shanab and K Adwan. Antibacterial activities of some plant extracts alone and in combination with different antimicrobials against multidrug-resistant *Pseudomonas aeruginosa* strains. *Asian Pacific Journal of Tropical Medicine* 2010; **3(4)**, 266-269.

[29] GD Nugroho, M Wiraatmaja, PS Pramadaningtyas, S Febriyanti, N Liza, DM Naim, YI Ulumuddin and A Setyawan. Review: Phytochemical composition, medicinal uses and other utilization of *Nypa fruticans*. *International Journal of Bonorowo Wetlands* 2020; **10(1)**, 51-65.

[30] F Martin, NS Boris, SR Kengne, TE Chia, TN Guy, AKB Gabin, JL Ngondi and G Innocent. Antioxidant and postprandial glucose-lowering potential of the hydroethanolic extract of *Nypa fruticans* seed mesocarp. *Biology and Medicine* 2017; **9(4)**, 1000407.

[31] MF Lubis, S Sumaiyah, LD Lubis, K Fitri and R Astyka. Application of Box-Behnken design for optimization of *Vernonia amygdalina* stem bark extract in relation to its antioxidant and anti-colon cancer activity. *Arabian Journal of Chemistry* 2024; **17(4)**, 105702.

[32] Y Fitri, Y Yusni, T Suryadi and M Mudatsir. Characteristic and bioactivities value of *Nypa fruticans* from coastal area in West Aceh District, Indonesia as a candidate antidiabetic agent. *Biodiversitas* 2023; **24(10)**, 5260-5269.

[33] N Moonrungsee, J Jakmunee, N Peamaroon, A Boonmee, T Kasemsuk, S Seeda and S Suwancharoen. Phytochemical and xanthine oxidase inhibitory activity in *Nypa fruticans* Wurmb. fruit extracts. *Trends in Sciences* 2022; **19(4)**, 2583.

[34] N Prasad, B Yang, KW Kong, HE Khoo, J Sun, A Azlan, A Ismail and ZB Romli. Phytochemicals and antioxidant capacity from *Nypa fruticans* Wurmb. Fruit. *Evidence-Based Complementary and Alternative Medicine* 2013; **2013**, 154606.

[35] N Chamkouri, Z Koolivand, F Niazvand and A Mojaddami. Phytochemical analysis, characterization, and biosynthesis of gold nanoparticles, zinc oxide nanoparticles, and gold-zinc oxide nanocomposites from *phoenix dactylifera L. seeds*: Biological evaluation. *Inorganic Chemistry Communications* 2023; **156**, 111146.

[36] R Sharma, N Kumar, P Sharma, A Yadav and NK Aggarwal. Biosynthesis, characterisation and therapeutic potential of green coconut waste derived zinc oxide nanoparticles. *Results in Surfaces and Interfaces* 2025; **18**, 100372.

[37] J Gangwar, B Balasubramanian, AP Singh, A Meyyazhagan, M Pappuswamy, AM Alanazi, KRR Rengasamy and JK Sebastian. Biosynthesis of zinc oxide nanoparticles mediated by *Strobilanthes hamiltoniana*: Characterizations, and its biological applications. *Kuwait Journal of Science* 2024; **51(1)**, 100102.

[38] D Suresh, PC Nethravathi, Udayabhanu, H Rajanaika, H Nagabhushana and SC Sharma. Green synthesis of multifunctional zinc oxide (ZnO) nanoparticles using *Cassia fistula* plant extract and their photodegradative, antioxidant and antibacterial activities. *Materials Science in Semiconductor Processing* 2015; **31**, 446-454.

[39] HM Yusof, NAA Rahman, R Mohamad, UH Zaidan and AA Samsudin. Optimization of biosynthesis zinc oxide nanoparticles: Desirability-function based response surface methodology, physicochemical characteristics, and its antioxidant properties. *OpenNano* 2022; **8**, 100106.

[40] N Jomehzadeh, Z Koolivand, E Dahdouh, A Akbari, A Zahedi and N Chamkouri. Investigating *in-vitro* antimicrobial activity, biosynthesis, and characterization of silver nanoparticles, zinc oxide nanoparticles, and silver-zinc oxide nanocomposites using *Pistacia Atlantica Resin*. *Materials Today Communications* 2021; **27**, 102457.

[41] H Mirzaei and M Darroudi. Zinc oxide nanoparticles: Biological synthesis and biomedical applications. *Ceramics International* 2017; **43(1)**, 907-914.

[42] A Mohammadi, N Hashemi, M Ghassabzadeh, A Sharafi, A Yazdinezhad and H Danafar. Green synthesis and toxicological evaluation of zinc oxide nanoparticles utilizing *Punica granatum* fruit Peel extract: An eco-friendly approach. *Scientific Reports* 2025; **15**, 20853.

[43] DR Jaishi, I Ojha, G Bhattarai, R Baraili, I Pathak, DR Ojha, DK Shrestha and KR Sharma. Plant-mediated synthesis of zinc oxide (ZnO) nanoparticles using *Alnus nepalensis* D. Don for biological applications. *Heliyon* 2024; **10(20)**, 39255.

[44] A Jayachandran, TR Aswathy and AS Nair. Green synthesis and characterization of zinc oxide nanoparticles using Cayratia pedata leaf extract. *Biochemistry and Biophysics Reports* 2021; **26**, 100995.

[45] A Raja, S Ashokkumar, RP Marthandam, J Jayachandiran, CP Khatiwada, K Kaviyarasu, RG Raman and M Swaminathan. Eco-friendly preparation of zinc oxide nanoparticles using *Tabernaemontana divaricata* and its photocatalytic and antimicrobial activity. *Journal of Photochemistry and Photobiology B: Biology* 2018; **181**, 53-58.

[46] AR Maheo, BSM Vithiya and TAA Prasad. Biosynthesis of chitosan and *Eupatorium adenophorum* mediated zinc oxide nanoparticles and their biological and photocatalytic activities. *Materials Today: Proceedings* 2022; **65(1)**, 298-312.

[47] YA Selim, MA Azb, I Ragab and MHMA El-Azim. Green synthesis of zinc oxide nanoparticles using aqueous extract of *Deverra tortuosa* and their Cytotoxic Activities. *Scientific Reports* 2020; **10**, 3445.

[48] AU Khan, N Malik, B Singh, NH Ansari, M Rehman and A Yadav. Biosynthesis, and characterization of Zinc oxide nanoparticles (ZnONPs) obtained from the extract of waste of strawberry. *Journal of Umm Al-Qura University for Applied Sciences* 2023; **9**, 268-275.

[49] TUD Thi, TT Nguyen, YD Thi, KHT Thi, BT Phan and KN Pham. Green synthesis of ZnO nanoparticles using orange fruit peel extract for antibacterial activities. *RSC Advances* 2020; **10(40)**, 23899-23907.

[50] RS Dangana, RC George and FK Agboola. The biosynthesis of zinc oxide nanoparticles using aqueous leaf extracts of *Cnidoscolus aconitifolius*

and their biological activities. *Green Chemistry Letters and Reviews* 2023; **16(1)**, 2169591.

[51] RK Rusli, M Hilmi, ME Mahata, A Yuniza, Z Zurmiati, S Reski, R Mutia and C Hidayat. Green synthesis of zinc oxide nanoparticles utilizing extract from Garcinia mangostana leaves: Characterization and optimization of calcination temperature. *Journal of Advanced Veterinary and Animal Research* 2024; **11(3)**, 573-582.

[52] NA Hussien, MAEF Khalil, M Schagerl and SS Ali. Green synthesis of zinc oxide nanoparticles as a promising nanomedicine approach for anticancer, antibacterial, and anti-inflammatory therapies. *International Journal of Nanomedicine* 2025; **20**, 4299-4317.

[53] S Faisal, H Jan, SA Shah, S Shah, A Khan, MT Akbar, M Rizwan, F Jan, Wajidullah, N Akhtar, A Khattak and S Syed. Green synthesis of zinc oxide (ZnO) nanoparticles using aqueous fruit extracts of *Myristica fragrans*: Their characterizations and biological and environmental applications. *ACS Omega* 2021; **6(14)**, 9709-9722.

[54] Z Wang, C Tang, X Mi, D Yao, Z Chen, C Guo, Y Zhao, X Xue, W Chang and Y Li. Zinc oxide nanoparticles alleviated vanadium-induced inhibition by regulating plant hormone signal transduction and phenylpropanoid biosynthesis in maize seedlings (*Zea may* L.). *Environmental Technology & Innovation* 2024; **35**, 103696.

[55] W Ibrahim, Muhlisin, Zuprizal and R Martien. Green synthesis of zinc nanoparticles using bioreductor from *Azadirachta indica* extract and its characteristics. *Indonesian Journal of Pharmacy* 2025; **36(2)**, 286-298.

[56] DN Mishra, L Prasad and U Suyal. Synthesis of zinc oxide nanoparticles using *Trichoderma harzianum* and its bio-efficacy on *Alternaria brassicae*. *Frontiers in Microbiology* 2025; **16**, 1506695.

[57] D Jain, Shivani, AA Bhojiya, H Singh, HK Daima, M Singh, SR Mohanty, BJ Stephen and A Singh. Microbial fabrication of zinc oxide nanoparticles and evaluation of their antimicrobial and photocatalytic properties. *Frontiers in Chemistry* 2020; **8**, 00778

[58] H Hamrayev, SD Jazayeri, M Yusefi, Brianna, SY Teow, YS Wu, A Anwar, S Korpayev, A Kartouzian and K Shameli. Green chemical approach for the synthesis of ZnO nanoparticles and investigation of their cytotoxicity. *Particle and Particle Systems Characterization* 2024; **41(8)**, 2400009.

[59] AR Mendes, CM Granadeiro, A Leite, O Geiss, I Bianchi, J Ponti, D Mehn, E Pereira, P Teixeira, and F Pocas. Functional properties and safety considerations of zinc oxide nanoparticles under varying conditions. *Nanomaterials* 2025; **15(12)**, 892.

[60] FH Abdullah, NHHA Bakar and MA Bakar. Low temperature biosynthesis of crystalline zinc oxide nanoparticles from *Musa acuminata* peel extract for visible-light degradation of methylene blue. *Optik* 2020; **206**, 164279.

[61] AE Alprol, A Eleryan, A Abouelwafa, AM Gad and TM Hamad. Green synthesis of zinc oxide nanoparticles using *Padina pavonica* extract for efficient photocatalytic removal of methylene blue. *Scientific Reports* 2024; **14**, 32160.

[62] M Mahajan, S Kumar, J Gaur, S Kaushal, J Dalal, G Singh, M Misra and DS Ahlawat. Green synthesis of ZnO nanoparticles using *Justicia adhatoda* for photocatalytic degradation of malachite green and reduction of 4-nitrophenol. *RSC Advances* 2025; **15(4)**, 2958-2980.

[63] S Zhou, R Liu, X Ma, Y Xie, X Xu, Q Du and Z Zhou. Antibacterial effect of novel dental resin composites containing rod-like zinc oxide. *Nanotechnology Reviews* 2024; **13**, 20230195.

[64] A Bharathi, R Meena, D Ravichandran, D Natarajan, MK Gatasheh, A Ahamed, R Kawuri and S Murugesan. Green route to synthesize zinc oxide nanoparticles (ZnO-NPs) using leaf extracts of *Merremia quinquefolia* (L.) Hallier f. and their potential applications. *Journal of Molecular Structure* 2024; **1317**, 139110.

[65] BL da Silva, MP Abuçafy, EB Manaia, JAO Junior, BG Chiari-Andréo, RCLR Pietro and LA Chiavacci. Relationship between structure and antimicrobial activity of zinc oxide nanoparticles: An overview. *International Journal of Nanomedicine* 2019; **14**, 9395-9410.

[66] MG Demissie, FK Sabir, GD Edossa and BA Gonfa. Synthesis of zinc oxide nanoparticles using leaf extract of *Lippia adoensis* (Koseret) and evaluation of its antibacterial activity. *Journal of Chemistry* 2020; **2020**, 7459042.

[67] MA Abomuti, EY Danish, A Firoz, N Hasan and MA Malik. Green synthesis of zinc oxide nanoparticles using *Salvia officinalis* leaf extract and their photocatalytic and antifungal activities. *Biology* 2021; **10(11)**, 1075.

[68] S Azizi, MM Shahri and R Mohamad. Green synthesis of zinc oxide nanoparticles for enhanced adsorption of lead Ions from aqueous solutions: Equilibrium, kinetic and thermodynamic studies. *Molecules* 2017; **22(6)**, 831.

[69] PC Nagajyothi, SJ Cha, IJ Yang, TVM Sreekanth, KJ Kim and HM Shin. Antioxidant and anti-inflammatory activities of zinc oxide nanoparticles synthesized using *Polygala tenuifolia* root extract. *Journal of Photochemistry and Photobiology B: Biology* 2015; **146**, 10-17.

[70] HB Boppudi, YS Rao, C Kuchi, AR Babu, V Govinda, M Jagadeesh and M Lavanya. Zinc oxide nanoparticles as an efficient antioxidant, photocatalyst, and heterogeneous catalyst in C–P bond synthesis. *Results in Chemistry* 2023; **6**, 101227.

[71] MS Almuhayawi, MH Alruhaili, MKY Soliman, MK Tarabulsi, RA Ashy, AA Saddiq, S Selim, Y Alruwaili and SS Salem. Investigating the *in vitro* antibacterial, antibiofilm, antioxidant, anticancer and antiviral activities of zinc oxide nanoparticles biofabricated from *Cassia javanica*. *PLoS One* 2024; **19(10)**, 0310927.

[72] MC Jobe, DMN Mthiyane, M Mwanza and DC Onwudiwe. Biosynthesis of zinc oxide and silver/zinc oxide nanoparticles from *Urginea epigea* for antibacterial and antioxidant applications. *Heliyon* 2022; **8(12)**, 12243.

[73] SA Neamah, S Albukhaty, IQ Falih, YH Dewir and HB Mahood. Biosynthesis of zinc oxide nanoparticles using *Capparis spinosa* L. fruit extract: Characterization, biocompatibility, and antioxidant activity. *Applied Sciences* 2023; **13(11)**, 6604.

[74] V Goyal, A Singh, J Singh, T Singh, AA Al-Kheraif, H Kaur, S Kumar and M Rawat. Biosynthesized zinc oxide nanoparticles as efficient photocatalytic and antimicrobial agent. *Journal of Cluster Science* 2022; **33**, 2551-2558.

[75] A Happy, M Soumya, SV Kumar, S Rajeshkumar, NDS Rani, T Lakshmi and VD Nallaswamy. Phyto-assisted synthesis of zinc oxide nanoparticles using *Cassia alata* and its antibacterial activity against *Escherichia coli*. *Biochemistry and Biophysics Reports* 2019; **17**, 208-211.

[76] M Irfan, H Munir and H Ismail. Moringa oleifera gum based silver and zinc oxide nanoparticles: Green synthesis, characterization and their antibacterial potential against MRSA. *Biomaterials Research* 2021; **25**, 17.

[77] Z Obeizi, H Benbouzid, S Ouchenane, D Yılmaz, M Culha and M Bououdina. Biosynthesis of zinc oxide nanoparticles from essential oil of *Eucalyptus globulus* with antimicrobial and anti-biofilm activities. *Materials Today Communications* 2020; **25**, 101553.

[78] A Abdelghafar, N Yousef and M Askoura. Zinc oxide nanoparticles reduce biofilm formation, synergize antibiotics action and attenuate *Staphylococcus aureus* virulence in host; an important message to clinicians. *BMC Microbiology* 2022; **22**, 244.

[79] G Chackaravarthy, NS Alharbi, M Gnanamangai, R Govindan, CK Chelliah, G Rajivgandhi, M Maruthupandy, F Quero, N Manoharan and WJ Li. Anti-biofilm efficacy of marine actinomycete mediated zinc oxide nanoparticles increased the intracellular damages in biofilm forming K. pneumoniae. *Journal of King Saud University - Science* 2023; **35(4)**, 102642.

[80] PK Jha, C Pokhum, P Soison, KA Techato and C Chawengkijwanich. Comparative study of zinc oxide nanocomposites with different noble metals synthesized by biological method for photocatalytic disinfection of Escherichia coli present in hospital wastewater. *Water Science and Technology* 2023; **88(6)**, 1564-1577.

[81] R Pati, RK Mehta, S Mohanty, A Padhi, M Sengupta, B Vaseeharan, C Goswami and A Sonawane. Topical application of zinc oxide nanoparticles reduces bacterial skin infection in mice and exhibits antibacterial activity by inducing oxidative stress response and cell membrane disintegration in macrophages. *Nanomedicine* 2014; **10(6)**, 1195-1208.